

In Situ Observation Reveals Local Detachment Mechanisms and Suction Effects in Micropatterned Adhesives

Verena Tinnemann, Luissé Hernández, Sarah C. L. Fischer, Eduard Arzt, Roland Bennewitz, and René Hensel*

Fibrillar adhesion pads of insects and geckoes have inspired the design of high-performance adhesives enabling a new generation of handling devices. Despite much progress over the last decade, the current understanding of these adhesives is limited to single contact pillars and the behavior of whole arrays is largely unexplored. In the study reported here, a novel approach is taken to gain insight into the detachment mechanisms of whole micropatterned arrays. Individual contacts are imaged by frustrated total internal reflection, allowing in situ observation of contact formation and separation during adhesion tests. The detachment of arrays is found to be governed by the distributed adhesion strength of individual pillars, but no collaborative effect mediated by elastic interactions can be detected. At the maximal force, about 30% of the mushroom structures are already detached. The adhesive forces decrease with reduced air pressure by 20% for the smooth and by 6% for the rough specimen. These contributions are attributed to a suction effect, whose strength depends critically on interfacial defects controlling the sealing quality of the contact. This dominates the detachment process and the resulting adhesion strength.

research for handling fragile and miniaturized objects, even in demanding environments such as vacuum.^[2–7] Among the various designs,^[8–11] microstructures with mushroom-shaped tips have an exceptionally high adhesion.^[12–14] It was demonstrated that their pull-off force, i.e., the force necessary for detaching the adhesive from a substrate, was up to an order of magnitude higher than with non-optimized flat punch pillars.^[10,15–18] The adhesion improvement was theoretically associated with a reduction of the stress singularities at the edges of the adhesive contact.^[19–22] Furthermore, it was found that the interfacial stress distribution affects the detachment mechanism because crack nucleation and propagation are controlled by local stresses.^[19,23] Heepe et al. studied the crack propagation of individual mushroom-shaped microstructures

1. Introduction

Innovative pick-and-place technologies are of great interest for advanced industrial automation processes.^[1] Inspired by the unique properties of adhesive surfaces found in nature, micropatterned adhesives are currently under intense


using a high-speed camera.^[17] They reported that the detachment was induced mainly by center cracks, i.e., penny-shaped cracks radially growing from an interfacial cavity toward the edge of the contact. Even in repeated adhesion experiments, interfacial cracks nucleated at the same preexisting interfacial defects. Most of the experimental and theoretical studies on the role of tip geometries were conducted using single pillar structures, which excludes additional effects such as elastic coupling between adjacent pillars through the backing layer or possible variations in the adhesive strength across the array.^[24–27]

The contribution of suction to adhesion of mushroom-shaped microstructures has been the subject of controversy. Davies et al. reported 25% suction contributing to adhesion of mushroom-shaped microstructures with tip diameters of 8 μm .^[28] In contrast, Henrey et al. reported no suction effect when comparing adhesion experiments at 10^{-5} mbar and atmospheric pressure.^[29] Similarly, Sameoto et al. reported that the suction effect was negligible for structures with tip diameters less than 17 μm .^[30] They proposed that mushroom tips with heads much larger than the stalk diameter could benefit from suction due to the enhanced probability of creating center cracks as a prerequisite for suction. For microstructures with a tip diameter of 50 μm , Heepe et al. reported a suction contribution of 10% which depended on the retraction velocity.^[31] They argued that air entered the contact at lower velocities due to imperfect sealing and thus reduced the pressure difference. Purto et al. studied switchable adhesives in vacuum using microstructures with tip diameters of about 600 μm .^[4] They obtained a high suction component of about

V. Tinnemann, L. Hernández, Dr. S. C. L. Fischer, Prof. E. Arzt, Prof. R. Bennewitz, Dr. R. Hensel
INM—Leibniz Institute for New Materials
Campus D2 2, 66123 Saarbrücken, Germany
E-mail: rene.hensel@leibniz-inm.de

V. Tinnemann, Prof. R. Bennewitz
Department of Physics
Saarland University
66123 Saarbrücken, Germany

Dr. S. C. L. Fischer, Prof. E. Arzt
Department of Materials Science and Engineering
Saarland University
66123 Saarbrücken, Germany

 The ORCID identification number(s) for the author(s) of this article can be found under <https://doi.org/10.1002/adfm.201807713>.

© 2019 The Authors. Published by WILEY-VCH Verlag GmbH & Co. KGaA, Weinheim. This is an open access article under the terms of the Creative Commons Attribution-NonCommercial-NoDerivs License, which permits use and distribution in any medium, provided the original work is properly cited, the use is non-commercial and no modifications or adaptations are made.

The copyright line was changed on 5 March 2019 after initial publication.

DOI: 10.1002/adfm.201807713

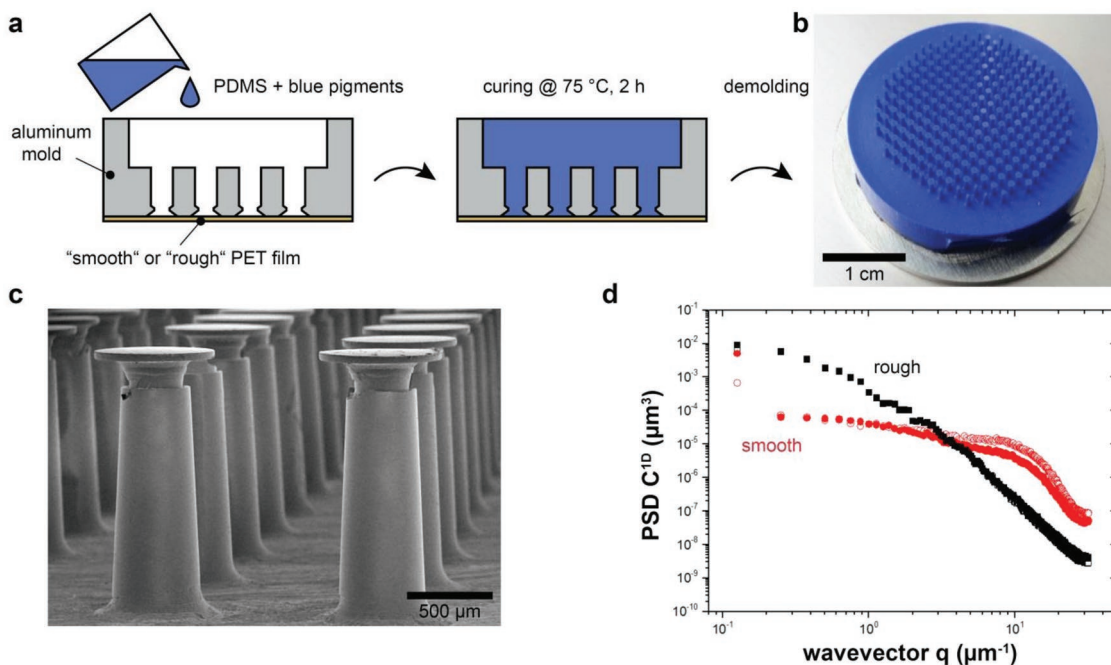


Figure 1. Fabrication and characterization of mushroom-shaped microstructures. a) Schematic illustration of the molding process: A polydimethylsiloxane (PDMS) prepolymer together with blue pigment is filled into an aluminum mold. The bottom of the mold was closed with a smooth or rough PET film. b) Optical image showing the dimensions of the micropatterned specimen. c) Electron image showing a side view of the mushroom shaped microstructures. d) Root mean squared height (h_{rms}) of the height distribution on the surfaces of the smooth and rough mushroom tips. Filled and unfilled symbols correspond to two different positions at the tip faces.

30%. This strong contribution may be related to the larger size of the mushroom tip compared to the other reports, although the contribution of suction to adhesion is of the same order of magnitude as that reported by Davies et al. for much smaller structures.^[28]

In the present paper, we investigate the detachment mechanisms of single mushroom shaped micropillars in adhesive arrays and their contribution to the array detachment. We established an optical microscopy method based on frustrated total internal reflection to detect contact of individual pillars with the substrate and to identify crack types during detachment experiments. Simultaneously recorded forces were correlated with the number of pillars in contact. Experiments were additionally performed at varying air pressure in order to clarify the role of suction.

2. Materials and Methods

2.1. Fabrication of Micropatterned Adhesives

Micropatterned dry adhesives were made from polydimethylsiloxane (PDMS, Sylgard 184, Dow Corning, Midland, MI, USA) via replica molding.^[32,33] The micropatterned arrays consisted of 236 mushroom-shaped pillars with a height of about 1600 μm , a stalk diameter of 400 μm , and a cap diameter of about 710 μm (see Figure 1c). The center-to-center distance was 1340 μm and the areal fraction of the contact area was 22%. The backing layer thickness was 5 mm. The PDMS was mixed in a 10:1 ratio of base and curing agent. For better optical contrast, 10 wt% blue pigments (PK 5091, Degussa, Essen Germany)

were added to the prepolymer. The components were mixed with 2350 rpm and degassed at 1 mbar for 3 min using a Speed-Mixer (DAC600.2 VAC-P, Hauschild Engineering, Hamm, Germany). For replica molding, an aluminum mold with milled microscopic holes (negative of the mushroom structure) was used as template (see Figure 1a). The bottom of the mold was closed by smooth or rough polyethylene terephthalate (PET) films. Specimens designated as “smooth” were replicated using a mold with PET film Melinex 401 CW (DuPont, Neu Isenburg, Germany), specimens designated as “rough” using a mold with PET laminating film Sigma (SIG GmbH, Düsseldorf, Germany). The surface roughness of the PET films was transferred to tips of the mushroom shaped microstructures. For this, the prepolymer mixture was filled into the mold and degassed for 5 min at 1 mbar. The mold was then closed with a lid to obtain a flat backing layer with a constant thickness of about 5 mm for all specimens. Finally, the prepolymer mixture was cured at 75 °C for 2 h. The surface roughness of the mushroom tips (related to the different PET films) was determined by 50 $\mu\text{m} \times 50 \mu\text{m}$ surface scans using an atomic force microscope. The topography data obtained were evaluated using the Surface Topography Analyzer developed by Lars Pastewka, Karlsruhe Institute of Technology, Germany (<http://contact.engineering/>) (see Figure 1d).^[34]

2.2. Adhesion Tests

Adhesion tests were performed with a tensile tester (Inspekt table BLUE, Hegewald&Peschke, Nossen, Germany)

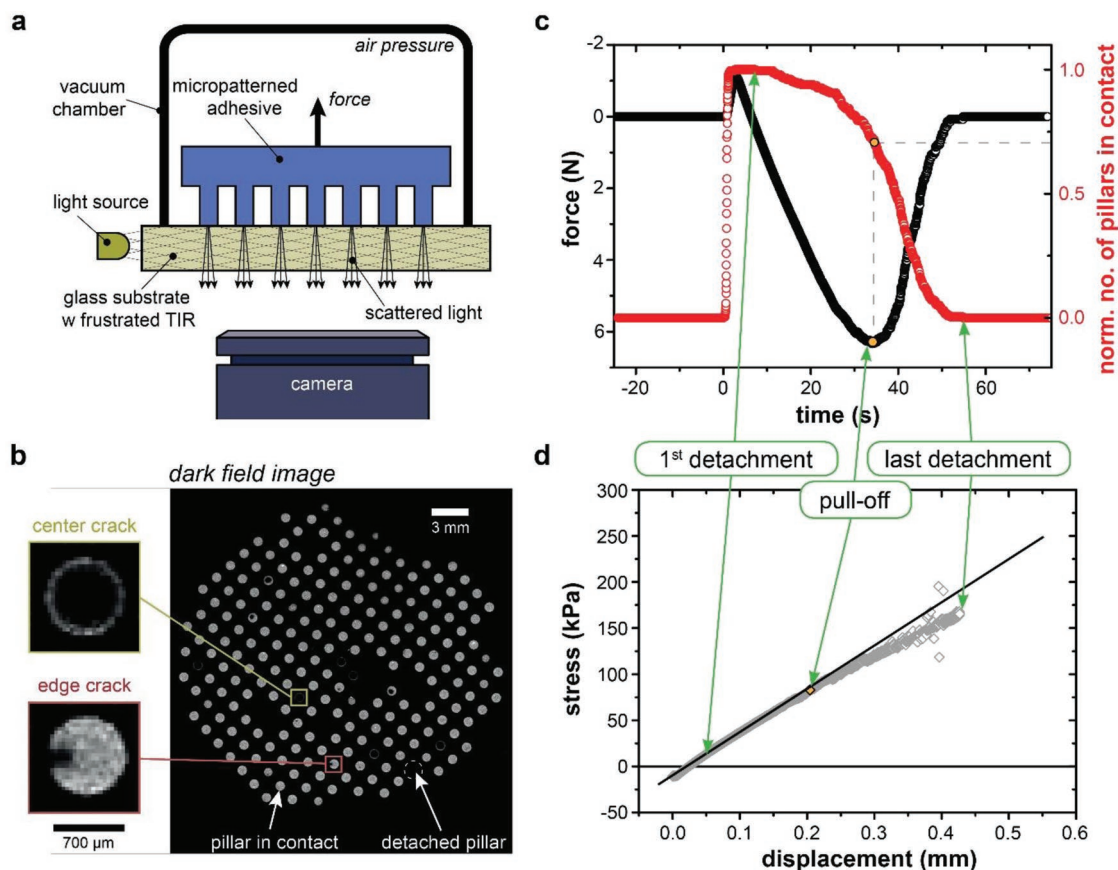


Figure 2. Adhesion test with in situ observation of attachment and detachment. a) Schematic illustration of the experimental setup. A micropatterned specimen (blue) is brought into contact with a nominally flat glass substrate. The principle of frustrated total internal reflection is used to visualize the individual contacts: Light is scattered only from areas of contact between pillars and substrate. The specimen and the load cell are mounted in a vacuum chamber. b) Dark field image representing individual contacts of the specimen with the substrate. The insets represent two crack types leading to detachment. c) Correlation of the adhesion force (black circles) and the normalized number of pillars in contact (red circles). The dashed line highlights the number of pillars in contact at the maximum adhesive force, i.e., the pull-off force. d) Stress versus displacement. Stress was calculated as the force per geometrical contact area, i.e., the number of pillar in contact multiplied with the top area of one mushroom structure. The orange dot indicates the displacement at which the maximum adhesive force was reached. The straight solid line serves as a guide to the eye and reveals a deviation from linear increase of stress. c,d) Data from an adhesion test of the smooth specimen at atmospheric pressure with a retraction velocity of 0.5 mm min^{-1} . Compressive forces and tensile stresses are plotted as positive values.

equipped with a 50 N load cell. The tensile tester was modified to perform adhesion tests on a smooth and nominally flat glass substrate at varying air pressure (see Figure 2a). A mirror and a camera were mounted below the transparent glass substrate which was connected to a θ - ϕ -goniometer (MOGO, Owis, Staufen im Breisgau, Germany) in order to align the substrate with the specimen. The contact of each pillar with the substrate was visualized in situ by the principle of frustrated total internal reflection (frustrated-TIR) as schematically shown in Figure 2a: Light (LEDs, YULED Everen, Lindlar, Germany) was coupled into the glass substrate (thickness of 10 mm) through its side walls and was subjected to total internal reflection at the glass–air interface.^[35–37] When a pillar formed contact with the substrate, the light was scattered at the substrate–pillar interface, appearing as a bright spot (see Figure 2b). Movies recorded of these spots revealed contact formation and detachment of each individual mushroom-shaped structure in the entire array. In addition, the crack types leading to detachment were identified. Image sequences and movies were recorded

using a digital camera (DMK33GX236, Imaging Source Europe GmbH, Bremen, Germany) with a resolution of $1920 \times 1200 \text{ pix}$ and a frame rate of 50 fps. The specimen and the load cell were mounted in a vacuum chamber consisting of a corrugated tube sealed with a gasket on the glass substrate. Experiments were performed from ambient air pressure (1000 mbar) down to 1 mbar. We accounted for the elastic deformation of the tensile tester by correcting the measured displacement for the machine compliance ($C = 7.43 \text{ } \mu\text{m mN}^{-1}$), a value which was found to be independent of the air pressure. In our study, the machine compliance was kept constant. It should be noted that a variation of the compliance may change the detachment characteristics.

In the adhesion measurements, specimen and substrate were brought together until a compressive preload of 1 N was reached. The velocity for contact formation (attachment) was always 1 mm min^{-1} . After reaching the preload, the specimen was immediately withdrawn until it detached from the substrate. The retraction velocity was varied between 0.5 and

10 mm min⁻¹. Measurements were repeated three times. Before each measurement, substrate and specimen were cleaned with isopropanol.

2.3. Image Analysis

Force–displacement data were correlated with image sequences as follows. Image sequences were binarized by threshold using Fiji^[38] such that contact (white) and noncontact (black) areas of mushroom pillars were identified. The x and y positions for each contact together with the time of attachment and detachment were determined using the Analyze Particle tool (Fiji). Position and time data were imported into a MATLAB routine (MathWorks, MA, USA) and correlated with force, time, and displacement data from the adhesion test. For synchronization, the image showing the detachment of the last pillar was attributed to the time when the tensile force relaxed to zero.

A second MATLAB routine was developed to determine different crack types. In the gray value image sequence, the center of gravity was determined for each contact. Onset of crack propagation was detected when gray values of individual pixels dropped over more than two images in a row. If the decrease of gray values occurred in pixels far from the center of gravity at a distance equal to the radius of the pillar (± 2 pixels), the crack was identified as an edge crack (see lower inset in Figure 2b). Cracks were identified as center cracks if the decrease of gray value occurred in pixels close to the center of gravity (see upper inset in Figure 2b).

3. Results

Mushroom-shaped microstructures were successfully produced by replica molding (Figure 1a). The polydimethylsiloxane specimens appeared blue due to the pigments added to the prepolymer mixture (Figure 1b). The pigments improved the contrast due to scattering of the totally reflected light when structures adhered to the substrate. The dimensions of the microstructures are confirmed in the electron image in Figure 1c. Mushroom tips were located at a tapered stalk with a diameter between 400 and 450 μm . The mushroom tip diameters were $710 \pm 15 \mu\text{m}$. Few pillars (less than 10%) did not exhibit complete mushroom tips mainly due to rupture during demolding. The mushroom-shaped pillars were organized in a square lattice array with a center-to-center distance of 1340 μm . The aluminum mold was closed at the bottom by a PET film that represented the counter surface during the fabrication. The film topography was replicated to the mushroom tip faces (see Figure 1a). Two PET films of different roughness were used. The power spectral density of the atomic force microscope height distribution is shown in Figure 1d.^[34] The roll-off wave vectors were about 15 and 2.5 μm^{-1} for the two specimens designated as “smooth” and “rough,” respectively. The Hurst exponents of both surfaces were about 1, indicating that the surface topographies were fractal.^[39] The root mean square height, h_{rms} , was about 20 nm for the smooth and almost twice that for the rough specimen with $h_{\text{rms}} = 37$ nm. For the smooth specimen, the root mean square slope was $h'_{\text{rms}} = 65$, whereas for the rough

specimen it was $h'_{\text{rms}} = 35$. Both specimens exhibited nanometer-scale surface roughness; the roughness of the “rough” sample was almost twice as high as that of the “smooth” sample.

Contact between tips and substrate caused light scattering only when the gap distance was less than half of the wavelength of the incident light, i.e., less than about 300 nm. Consequently, defects and cracks with corresponding opening could be observed (see insets in Figure 2b and Figure 5a). Figure 2c exemplifies the correlation of forces (black curve) with the normalized number of pillars in contact at each time step (red curve) during retraction of the specimen. All pillars were attached to the substrate at a set compressive preload of 1 N. All pillars were attached within an approach distance of 30 μm , i.e., only 2% of the pillar height, demonstrating the homogeneity of the samples and the success of the tilt correction. When the specimen was retracted at a velocity of 0.5 mm min⁻¹, a pull-off force, i.e., the maximum tensile force, of about 6 N was measured (orange dot in Figure 2c). However, individual pillars started to detach at lower tensile forces and 30% of the pillars were already released at the pull-off force, which is in line with earlier reports.^[40]

The normal stresses were determined by dividing the force by the geometrical contact area, i.e., the product of the number of pillars in contact and the top area of a single pillar (Figure 2d). The retraction started at the maximum compressive preload, i.e., maximum negative stress. First pillar detachment occurred at 20 kPa in the tensile regime. The stress increased almost linearly with increasing displacement, with a slightly decreasing slope. At “pull-off,” i.e., the global maximum tensile force (orange dot in Figure 2c,d), the stress of individual pillars in contact with the substrate was about 70 kPa. Upon passing pull-off, the stress further increased up to 160 kPa that corresponds to the adhesion strength of the strongest pillar. The significant scatter of the stress values just before final detachment at 160 kPa is related to the large errors in dividing by a vanishing geometrical contact area (Figure 2d). Considering the high degree of perfection of the sample demonstrated in the scanning electron microscope (SEM) images and in the small scatter in attachment height, we can conclude that there is a large difference in individual adhesion strength of the pillars varying from 20 to 160 kPa. This result contrasts with the common tacit assumption that all pillars of a specimen adhere with equal strength.

In order to investigate possible elastic interactions between pillars, **Figure 3** analyzes how many neighboring pillars were already detached when a given pillar was released from the surface. In the array, each pillar has eight neighbors, except for pillars located at the edge and the corner, where the minimum number of neighbors is five and three, respectively. Detachment always started at a pillar with zero detached neighbors and increased with ongoing detachment. Two limiting cases exist: i) A strong coupling between adjacent pillars by the elastic backing layer would induce a detachment wave which propagates through the entire array of pillars. In this case, each pillar would detach typically with four neighbors already detached as shown by the peak in the histogram (black bars) of Figure 3a and the constant number of four neighbors for the ongoing detachment process (black diamonds) in Figure 3b. ii) In the second limiting case no coupling between the pillars and random order of detachment is assumed. In this case, the

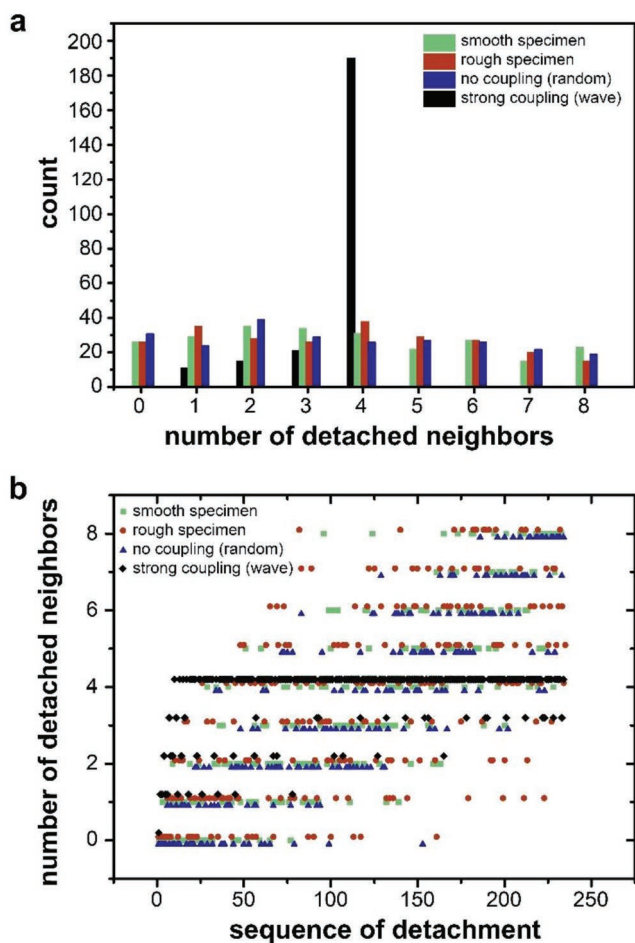


Figure 3. Influence of the number of previously detached neighbors on the detachment of individual pillars. a) Histogram showing the number of neighbors that are already separated from the substrate before a certain pillar detached. Data for experiments with the smooth (green) and rough (red) specimen are compared to two limiting cases which were modeled as random detachment without any coupling by the backing layer (blue) and as a detachment wave caused by strong coupling (black). b) Number of detached neighbors in the sequence of detachment for the smooth (green squares) and the rough (red dots) specimen compared to the two modeled limiting cases of strong (black diamonds) and no coupling (blue triangle). Both analyses were performed for a measurement at a retraction velocity of 10 mm min^{-1} and at atmospheric pressure.

number of detached neighbors would increase steadily from zero to eight with advancing detachment (brown triangles in Figure 3b), whereas the overall count would be evenly distributed between 20 and 40 (brown bars) for the different numbers of neighbors already detached (Figure 3a). The second limiting case is the one found experimentally for both the smooth (green) and rough (red) specimen. We conclude that the detachment for rough and smooth specimen proceeded in random order. The wide distribution of adhesive strength of individual pillars has by far stronger influence on the detachment process than possible correlation effects introduced by elastic coupling through the backing layer.

Results of adhesion tests at different air pressure are presented in Figure 4a, where the forces are plotted against the

normalized number of pillars in contact. The pull-off force decreased by 20% when the pressure was reduced from 1000 to 1 mbar and by 3.5% from 100 to 1 mbar for the smooth sample. Pull-off forces measured with rough specimens were much less sensitive to air pressure reduction with a decrease of the adhesion force by 6% from 1000 to 1 mbar. The pull-off force of the rough specimen was lower by one half to one third compared to the smooth specimen for all air pressures. The normalized number of pillars in contact at the pull-off force varied slightly between 0.75 and 0.70 for the smooth and rough specimen, respectively, and was found to be independent of the air pressure.

Note that the shapes of the curves in Figure 4a are similar, implying that the progress of pillar detachment is insensitive to air pressure. To prove this, the similarity of the sequence of pillar detachment for different air pressure was quantified: Pillars were consecutively indexed in the order they detached from the substrate at atmospheric pressure. The indices obtained from the measurements at 100 and 1 mbar were then subtracted from the initial sequence of detachment at 1000 mbar (Figure 4b,c). The standard deviation, sd , obtained for the different detachment sequences at various air pressures provides a measure of their similarity. For the smooth specimen, $sd = 0.11$ for 100 mbar compared to 1000 mbar and $sd = 0.12$ for 1 mbar compared to 1000 mbar. At reduced air pressure (1 mbar compared to 100 mbar), the detachment sequences were more similar with $sd = 0.04$. Higher standard deviations were obtained for the rough specimen: $sd = 0.21$ and $sd = 0.22$ for 100 and 1 mbar, respectively, compared to 1000 mbar. For 1 mbar compared to 100 mbar, the standard deviation was $sd = 0.10$.

In addition to the spatial and temporal analysis of pillars detaching from the substrate, the characteristic type of cracks was identified by in situ observation: i) Cracks that started at the edge and spread through the contact to the opposite edge are so-called “edge cracks” (red inset Figure 2b). ii) Cracks that nucleated centrally in the contact and grew radially from the inside to the outside are referred to as “center cracks” (brown inset Figure 2b). For a retraction velocity of 0.5 mm min^{-1} , the typical duration of crack propagation is summarized in Table 1. Irrespective of air pressure and surface roughness, edge cracks were always faster than center cracks with a mean propagation time between 20 and 80 ms; this corresponds to a crack propagation speed of up to 20 mm s^{-1} . In contrast, the mean propagation time of center cracks varied between 30 and 630 ms, which is also reflected in a difference of two orders of magnitude between the fastest (20 ms) and the slowest (5240 ms) center crack. Center cracks propagated faster by almost factor 6 with increasing surface roughness and by a factor 3 with reduction of the air pressure. Note that due to the temporal resolution of the camera the crack type could only be determined for propagation times above 20 ms, the time step between subsequent images. Cracks propagating in a detachment which took less than 20 ms were labeled as “fast.”

The propagation of center cracks was further analyzed by plotting the normalized mean gray value of individual pillar contacts over time (Figure 5a). Before and shortly after the pull-off event, center cracks grew in a characteristic manner as exemplarily shown for pillars #23 and #60: Upon nucleation,

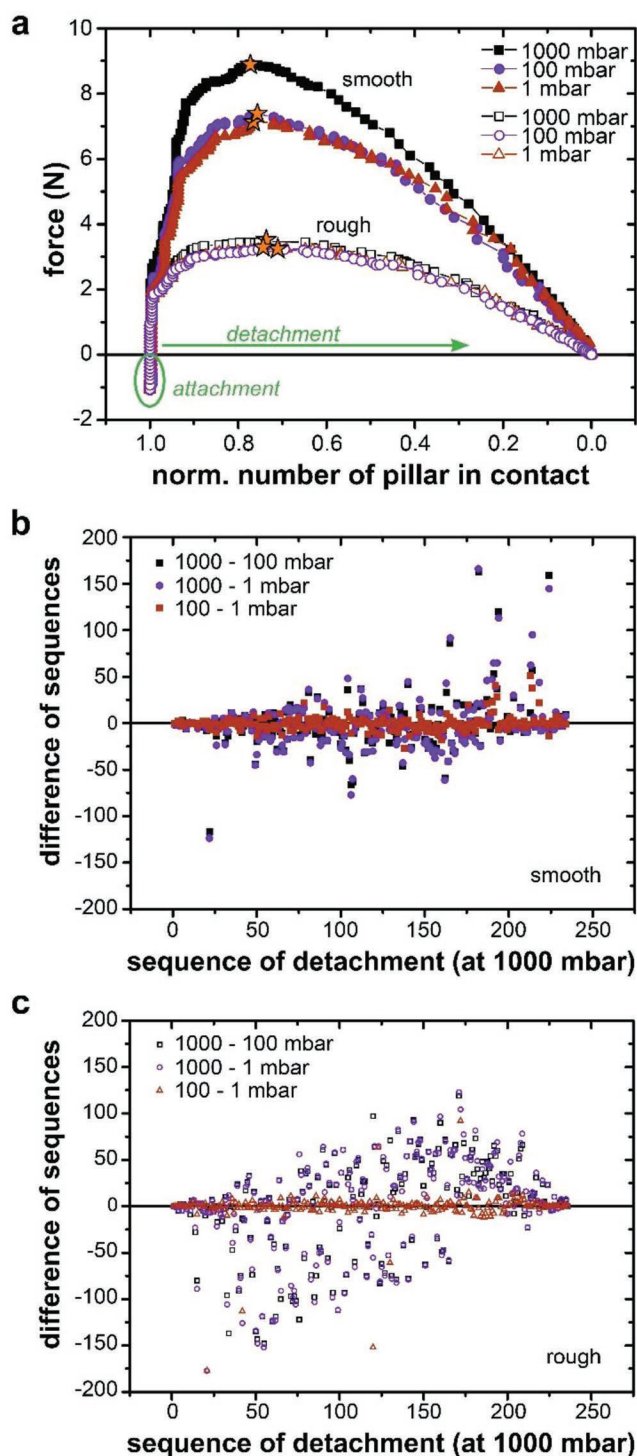


Figure 4. Results of the adhesion tests for mushroom pillars with smooth and rough tips at varying air pressures. a) Force as a function of normalized number of pillar in contact with the substrate. Negative and positive forces represent compressive and tensile forces, respectively. The filled and unfilled symbols correspond to structures with smooth and rough tips, respectively. The orange symbols highlight the pull-off force. The air pressure was varied from atmospheric pressure (black), 100 mbar (purple), and 1 mbar (red). The retraction velocity was 10 mm min^{-1} . Variation in the sequence of detachment between measurements at different air pressure for b) the smooth and c) the rough specimen. The difference

Table 1. Times for crack propagation of center and edge cracks for the a) smooth and b) the rough specimen at various air pressures. The times were calculated for all pillars that clearly detached via center or edge. The crack propagation times are presented as mean value (t_{mean}), standard deviation (t_{SD}), and maximum time (t_{max}). The retraction velocity was 0.5 mm min^{-1} .

Crack type	Air pressure [mbar]	t_{mean} [ms]	t_{SD} [ms]	t_{max} [ms]
a) Smooth specimen				
Center crack	1000	630	1020	5240
Edge crack		80	120	560
Center crack	100	170	500	2480
Edge crack		60	70	440
Center crack	1	120	420	2440
Edge crack		80	210	1580
b) Rough specimen				
Center crack	1000	100	110	580
Edge crack		80	120	320
Center crack	100	30	10	120
Edge crack		20	10	40
Center crack	1	30	20	140
Edge crack		20	10	40

the crack growth rate was high (about 2 mm s^{-1}) but then decreased drastically (see regions marked with green lines in Figure 5a). This deceleration occurred once the area below the stalk was detached while the rim of the mushroom tip still remained in contact (pillar #23 in Figure 5a). Over this period of up to 200 ms, the gray value decreased only slightly from 0.4 to about 0.2. This suggests that the cavity most probably grew in normal direction before detachment finally occurred. Note that the detachment of pillar #23 occurred before reaching the pull-off force of the array (dashed line), whereas all other pillars detached thereafter. Later in the detachment, beyond the pull-off event, center cracks propagated faster and continuously through the contact, accompanied by a steady decrease of the normalized mean gray value from 1 to 0 (pillars #125 and #234). The propagation times extracted from the videos are listed in Table 1. Only crack propagation times longer than 20 ms could be recorded. Cracks that were faster could not be detected in the video recordings.

In Figure 5b–e, the number of pillars with a crack propagating through the contact, for a given frame of the video, is plotted together with the force–time curve recorded during retraction of the specimen. We start by comparing results for the smooth specimen at atmospheric pressure (Figure 5b) and 1 mbar (Figure 5c). A large number of center cracks (up to 17) was observed simultaneously when reaching the pull-off force at atmospheric pressure, whereas only up to three center cracks propagated simultaneously at 1 mbar. The total number of center cracks decreased from 115 to 39 when reducing the

of the sequence of pillar detachment is calculated by subtracting the sequence for 100 mbar (black) or 1 mbar (red) from the sequence obtained for 1000 bar and subtracting the sequence for 1 mbar from 100 mbar (blue).

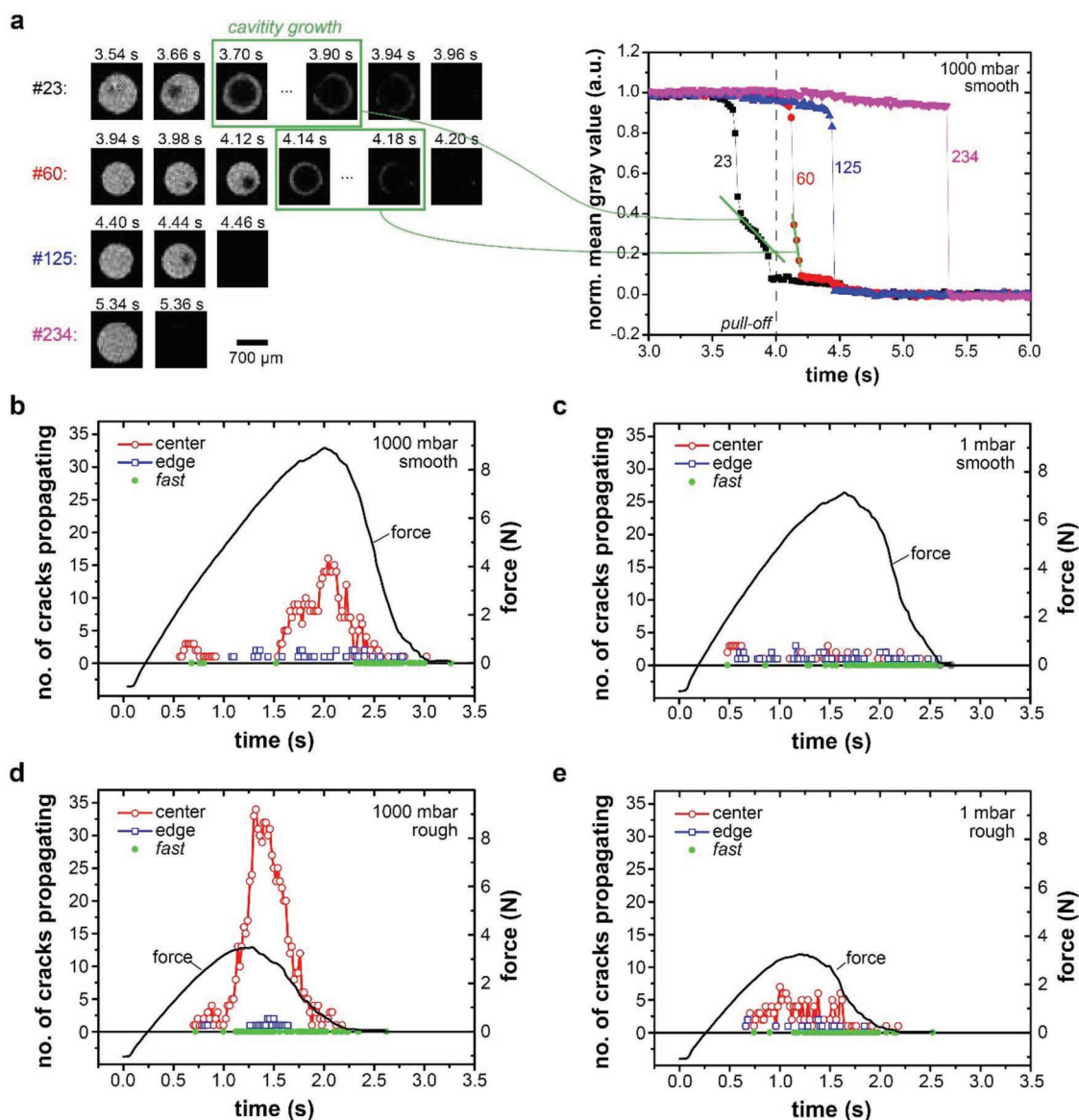


Figure 5. In situ crack analysis on a) the single pillar level and b–e) the entire array level. a) Image sequences of individual pillars detaching from the substrate. Pillar numbers correspond to the detachment order; the dashed vertical line marks the pull-off of the array. The evolution of the normalized mean gray values during detachment is shown on the right. The values 1 and 0 represent complete contact and the detached state, respectively. The cavity growth in normal direction is highlighted in green. b–e) The number of pillars with center cracks (red) and edge cracks (blue) simultaneously propagating at each time step of 20 ms (corresponding to individual video frames) as a function of time for the smooth specimen at b) atmospheric pressure and c) 1 mbar and for the rough specimen at d) atmospheric pressure and e) 1 mbar. The solid black line is the force–time curve. The retraction velocity was 10 mm min⁻¹. Cracks which propagated faster than 20 ms are labeled as “fast” cracks (green).

air pressure, whereas the total number of edge cracks slightly increased from 36 to 48 and the number of fast cracks increased from 83 to 147. Note that most of the fast cracks were observed toward the end of retraction after reaching the pull-off force. It should be noted that at the beginning of retraction (between 0.5 and 1 s) pillars with larger defects or missing mushroom tips were detached. The trends for the smooth specimen were similarly observed for the rough specimen. A large number of pillars with center cracks (up to 34) were observed simultaneously close to pull-off force at atmospheric pressure (Figure 5d), whereas this number drastically decreased at

1 mbar (Figure 5e). The total number of center cracks decreased from 159 to 113 when reducing the air pressure, a number still higher than for the smooth specimen. The number of edge cracks and fast cracks increased from 11 to 15 and from 64 to 107, respectively.

The contribution of suction to the adhesion strength of each individual pillar is shown in Figure 6. The adhesion strength of each pillar was estimated as the ratio of the total force, at the moment of its detachment, divided by the geometrical contact area, i.e., the number of pillars still in contact multiplied by the tip area of a mushroom. For 1000 mbar, the

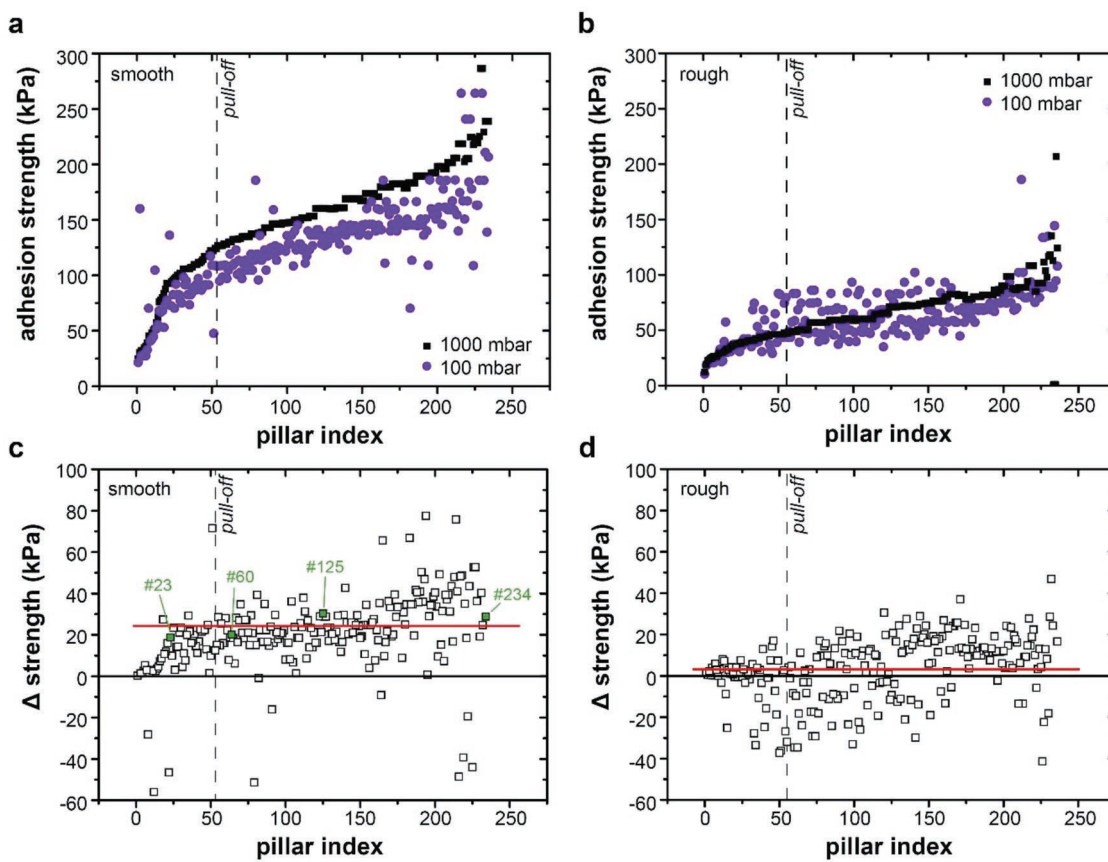


Figure 6. Suction contribution analysis. a,b) Adhesion strength of individual pillars at 1000 mbar (black) and 100 mbar (purple) for a) the smooth and b) the rough specimen, indexed by the sequence of detachment at 1000 mbar. Differences of the adhesion strength values caused by the different air pressures for each individual pillar of c) the smooth and d) the rough specimen. The green squares in (c) highlight the pillars shown in Figure 5a. The horizontal red lines represent the mean value. Dashed vertical lines highlight the reaching of the pull-off force.

strength continuously increased because the pillars were consecutively indexed during this experiment (Figure 6a,b). The strengths increased from 25 kPa to about 250 kPa for the smooth specimen and from 10 to 125 kPa for the rough specimen (black squares). For the smooth specimen, almost all pillars exhibited a smaller adhesion strength upon pressure reduction to 100 mbar (purple dots). Only a few pillars showed higher adhesion (Figure 6a). In contrast, for the rough specimen, a large fraction of pillars exhibited stronger adhesion upon pressure reduction (Figure 6b). The differences in strength of each individual pillar between 1000 and 100 mbar are shown in Figure 6c,d. For the smooth specimen, the strength differences varied between -60 and 80 kPa. The mean value was about 26 kPa as highlighted by the red line in Figure 6c. Thus, a higher fraction of pillars exhibited a positive stress difference, which is in line with the globally measured 20% difference of the pull-off force between atmospheric pressure and 100 mbar. Note that irrespective of the time for crack growth (see Figure 5a), the strength differences related to pressure variations can be similar as highlighted by the green squares in Figure 6c. For the rough specimen, the strength differences of the individual pillars varied between -50 and 50 kPa with a mean value of 3 kPa, being again similar to the macroscopically measured pull-off force reduction of 6%.

4. Discussion

Our combined approach of adhesion tests and in situ observation of the contact area provides entirely new insights into the performance and detachment characteristics of micropatterned dry adhesives. We found that, despite similar appearance of the mushroom-shaped pillars in SEM images, their individual adhesion strength varied strongly—by a factor of up to 10—within the same array. It is interesting to note that typically about 30% of the pillars were already detached when the array reached its pull-off force, i.e., the maximum adhesion force measured in the course of retraction of the whole sample.

Based on the wide spread of individual adhesion strength values, we suggest that the adhesion strength of individual pillars is controlled by interfacial defects which determine the critical stresses for crack formation. We did not observe preferential detachment of adjacent pillars, which could have been expected in the presence of elastic coupling through the backing layer (see Figure 3) as was theoretically predicted by Bacca et al.^[25] The location of the interfacial defects may depend on details of surface roughness of the pillars, structural inhomogeneities of the counter surface, and dust particles. These details also predetermined whether the crack propagated from the edge or from the center of the contact. The sequence

of pillar detachment was similar in experiments repeated at different air pressures, various retraction velocities (see Figure S1, Supporting Information), and repeated measurements at the same and different positions of the substrate (see Figure S2, Supporting Information). This predictability of the detachment sequence, however, was reduced with increasing roughness, which supports our conclusion of a defect-controlled detachment. It should be noted that mushroom tips were much rougher than the glass substrate; thus, interfacial defects including their size and local distribution were similar in the different tests. We suggest that for substrates being rougher than the pillar faces, the sequence of detachment most likely vary drastically due to the fact that interfacial defects will vary in each experiment.

The adhesion force varied as a function of air pressure. This indicates that suction contributes to adhesion. For the rough counter-surface, this contribution amounts to only about 6%, for the smooth counter-surface to about 20% (see Figure 4). A pressure difference leading to suction cannot be maintained in the presence of edge cracks but only by internal cavities that may eventually turn into center cracks. The number of center cracks alone could not explain the suction effect as suggested before.^[4,31] We found more center cracks for the rough than the smooth specimen (even if all fast cracks were defined as center cracks; see Figure 5b,d), although the suction contribution was smaller for the rough specimen. We therefore must invoke an additional mechanism responsible for a strong suction component. It stands to reason that the stable, vertical growth of a center cavity will decrease the internal air pressure and hence increase the suction effect. Stable cavity growth is supported by a strongly decelerated crack propagation toward the rim of the mushroom edge, which hence continues to seal the cavity. Such crack deceleration has been predicted by Afferrante and Carbone as a process comparable to the peeling of an axisymmetric membrane.^[41] In agreement with this picture, the cavity growth regime was identified by a slower decrease in the mean gray value over time in our movies and by the observation that the rim of the mushroom-shaped pillar stayed in contact with the counter-surface (see Figure 5a).

Cavity growth is not limited to conditions of slow crack propagation; large expansions can be realized also within short crack propagation times as is exemplarily shown for pillar #234 in Figure 5a. Cavity growth depends critically on elasticity. The shape of the cavity is a function of p/E , where p is the pressure inside the cavity and E the elastic modulus.^[42] For $p/E \approx 1$, cavities exhibit a hemispherical shape, while for $p/E \approx 0.05$ (with the suction limit of $p = 100$ kPa and $E = 2$ MPa for PDMS) it is much more prolate. Besides the formation of cavities, air leakage induced by interfacial defects can cause compensation of the pressure difference between inside and outside the cavity.^[43] This explains faster crack growth and significant lower suction component for the rough specimen, as increasing roughness affords larger interfacial defects due to incomplete adhesive contacts and a higher probability of percolations paths. Furthermore, roughness often implies incomplete contact and pre-existing cracks, which will propagate at a critical stress. Hence, rougher specimens exhibit a higher fraction of center cracks. It should be noted that this argument is valid for critical

crack sizes much smaller than the mushroom tip size as found in our experiments. For very thin pillars with critical defects in the same dimension as the contact area, the probability of edge crack detachment without any suction effect will increase.

Contrary to expectation, we found that a significant fraction of pillars adhered better under reduced compared to atmospheric pressure (see Figure 6). The random scatter of adhesion strengths in subsequent detachment experiments is hence larger than the small average suction increase of adhesion strength at reduced pressure, in particular for the rough specimen. The random scattering of individual contact strength depends on details of the contact formation and thus of the location and nature of interfacial defects. Small changes in the lateral position of the specimen with respect to the substrate between two measurements at different air pressure may lead to a quite different set of interfacial defects. This observation again supports the hypothesis that local defects control crack formation and cavity growth and, thus, the adhesive strength of individual pillars. Random variation of the defects then leads to increased adhesion strength for some pillars despite the overall average decrease in adhesion at reduced pressure.

To benefit from suction, the ratio of the mushroom cap diameter to the stalk diameter has to be large enough to maximize the probability of center crack detachment accompanied with the formation of cavities.^[19] As second prerequisite, interfacial defects should be small as possible in a way that air leakage is inhibited. Perfectly smooth surfaces of the microstructures and the substrate would therefore give best results. Microstructures made from softer materials may further support better adaptation to the surface topography and less air leakage. However, the reduction of the elastic modulus is typically associated with a decrease of the theoretical adhesion strength.^[1,44]

In general, the adhesive strength depends on the size of a critical defect, with larger defects being more critical to adhesion. Large defects can be eliminated by miniaturization of individual contacts that, in addition, would enhance the performance by reducing the stress concentrations at the contact edge.^[19] In the same way, the contribution by suction vanishes as it scales by area.^[45] However, it remains hypothetical how miniaturization of individual contacts would affect the distribution of adhesion strength. The size of the largest possible defect reduces, which enhances adhesion, but in turn, adhesion could become negligible for structures with similar dimensions of a defect.

5. Conclusions

An in situ method for visualizing individual contacts in micropatterned adhesive systems was employed to gain insight into mechanisms of the detachment process. The method successfully revealed gradual, noncollaborative detachment processes in the array of pillars and distinguished crack types occurring during detachment of individual pillars. The following conclusions can be drawn:

- The detachment process begins at forces far below the macroscopic pull-off force. A large fraction of pillars (up to 30% for the specimens tested) are already detached when the maximum tensile force is reached. The order of

individual detachments reflects the distribution of adhesion strength of the individual pillars, which is related to local defects in the interface between pillars and the counter-surface.

- No indications for significant collaborative effects due to elastic coupling between pillars were found. Such a coupling would have been expected for a homogeneous regular array of equal mushroom-shaped pillars with an elastic backing layer.
- The pull-off force varies characteristically with air pressure and retraction velocity, but the shape of the force-detachment curves remains very similar. Air-pressure and retraction velocity seem to have almost no influence on the sequence of pillar detachment.
- Center crack formation is a prerequisite for suction contributions to the adhesive strength. The growth of cavities leads to a pressure reduction, which increases adhesion through suction. The number of center cracks alone cannot predict the suction contribution since the expansion of the cavity varies greatly between pillars. The macroscopically measured suction contribution is rather the mean suction contribution of the individual pillars.
- Cavity growth is limited by interfacial defects which reduce the sealing quality of the attached mushroom rim. Therefore, incomplete contact due to roughness, dust particles, and so on limits the suction contribution of each pillar.

In summary, the approach presented in this work revealed that the adhesion strengths of the individual pillars were distributed over about one order of magnitude, though microscopy of the shape of the microstructures exhibited a high degree of perfection and similarity upon fabrication. We found that the variation in adhesion strength originates from interfacial defects of different size, being omnipresent in the adhesive contact. In addition, measurements at different air pressures allowed to quantify suction effects in micropatterned dry adhesives. We demonstrated that the suction contribution depends on air leakage into cavities being present in the adhesive contacts and is therefore also controlled by interfacial defects.

Supporting Information

Supporting Information is available from the Wiley Online Library or from the author.

Acknowledgements

The technique of total internal reflection was suggested to the authors by Mark Cutkosky, Stanford University. The authors thank Martin Schmitz, Werner Schneider, and Fabian Hüther for technical support and Wiebke Mary Buhrow for AFM measurements. In addition, the authors acknowledge Prof. Robert M. McMeeking and Jamie Booth (University of California Santa Barbara, CA, USA) for valuable discussions. The work was funded from the European Research Council (ERC) under the European Union's Seventh Framework Program (FP/2007-2013)/ERC Advanced Grant No. 340929.

Conflict of Interest

The authors declare no conflict of interest.

Keywords

adhesion, bioinspiration, elastic coupling, in-situ observation, micropatterning, suction

Received: November 1, 2018

Revised: December 18, 2018

Published online: January 31, 2019

- [1] R. Hensel, K. Moh, E. Arzt, *Adv. Funct. Mater.* **2018**, *28*, 1800865.
- [2] M. Zhou, Y. Tian, D. Sameoto, X. Zhang, Y. Meng, S. Wen, *ACS Appl. Mater. Interfaces* **2013**, *5*, 10137.
- [3] H. E. Jeong, J.-K. Lee, H. N. Kim, S. H. Moon, K. Y. Suh, *Proc. Natl. Acad. Sci. USA* **2009**, *106*, 5639.
- [4] J. Purto, M. Frensemeier, E. Kroner, *ACS Appl. Mater. Interfaces* **2015**, *7*, 24127.
- [5] S. Song, D.-M. Drotlef, C. Majidi, M. Sitti, *Proc. Natl. Acad. Sci. USA* **2017**, *114*, E4344.
- [6] Y. Y. Mengüç, S. Y. Yang, S. Kim, J. A. Rogers, M. Sitti, *Adv. Funct. Mater.* **2012**, *22*, 1246.
- [7] H. K. Minsky, K. T. Turner, *ACS Appl. Mater. Interfaces* **2017**, *9*, 18322.
- [8] S. C. L. Fischer, K. Groß, O. Torrents Abad, M. M. Becker, E. Park, R. Hensel, E. Arzt, *Adv. Mater. Interfaces* **2017**, *4*, 1700292.
- [9] S. C. L. Fischer, E. Arzt, R. Hensel, *ACS Appl. Mater. Interfaces* **2017**, *9*, 1036.
- [10] A. Del Campo, C. Greiner, E. Arzt, *Langmuir* **2007**, *23*, 10235.
- [11] H. K. Minsky, K. T. Turner, *Appl. Phys. Lett.* **2015**, *106*, 201604.
- [12] S. N. Gorb, M. Varenberg, *J. Adhes. Sci. Technol.* **2007**, *21*, 1175.
- [13] A. Del Campo, C. Greiner, I. Álvarez, E. Arzt, *Adv. Mater.* **2007**, *19*, 1973.
- [14] S. Kim, M. Sitti, *Appl. Phys. Lett.* **2006**, *89*, 261911.
- [15] L. Heepe, A. E. Kovalev, M. Varenberg, J. Tuma, S. N. Gorb, *Theor. Appl. Mech. Lett.* **2012**, *2*, 014008.
- [16] E. Kroner, E. Arzt, *Int. J. Adhes. Adhes.* **2012**, *36*, 32.
- [17] L. Heepe, A. E. Kovalev, A. E. Filippov, S. N. Gorb, *Phys. Rev. Lett.* **2013**, *111*, 104301.
- [18] E. P. Chan, C. Greiner, E. Arzt, A. J. Crosby, *MRS Bull.* **2007**, *32*, 496.
- [19] R. G. Balijepalli, M. R. Begley, N. A. Fleck, R. M. McMeeking, E. Arzt, *Int. J. Solids Struct.* **2016**, *85–86*, 160.
- [20] B. Aksak, K. Sahin, M. Sitti, *Beilstein J. Nanotechnol.* **2014**, *5*, 630.
- [21] G. Carbone, E. Pierro, *Small* **2012**, *8*, 1449.
- [22] A. V. Spuskanyuk, R. M. McMeeking, V. S. Deshpande, E. Arzt, *Acta Biomater.* **2008**, *4*, 1669.
- [23] R. G. Balijepalli, S. C. L. Fischer, R. Hensel, R. M. McMeeking, E. Arzt, *J. Mech. Phys. Solids* **2017**, *99*, 357.
- [24] S. Kim, M. Sitti, C.-Y. Hui, R. Long, A. Jagota, *Appl. Phys. Lett.* **2007**, *91*, 161905.
- [25] M. Bacca, J. A. Booth, K. L. Turner, R. M. McMeeking, *J. Mech. Phys. Solids* **2016**, *96*, 428.
- [26] R. Long, C.-Y. Hui, S. Kim, M. Sitti, *J. Appl. Phys.* **2008**, *104*, 044301.
- [27] G. M. Guidoni, D. Schillo, U. Hagen, G. Castellanos, E. Arzt, R. M. McMeeking, R. Bennewitz, *J. Mech. Phys. Solids* **2010**, *58*, 1571.
- [28] J. Davies, S. Haq, T. Hawke, J. P. Sargent, *Int. J. Adhes. Adhes.* **2009**, *29*, 380.
- [29] M. Henrey, J. P. Díaz Téllez, K. Wormnes, L. Pambaguian, C. Menon, *Aerosp. Sci. Technol.* **2013**, *29*, 185.
- [30] D. Sameoto, H. Sharif, C. Menon, *J. Adhes. Sci. Technol.* **2012**, *26*, 2641.

- [31] L. Heepe, M. Varenberg, Y. Itovich, S. N. Gorb, *J. R. Soc., Interface* **2011**, *8*, 585.
- [32] V. Barreau, R. Hensel, N. K. Guimard, A. Ghatak, R. M. McMeeking, E. Arzt, *Adv. Funct. Mater.* **2016**, *26*, 4687.
- [33] A. Finn, R. Hensel, F. Hagemann, R. Kirchner, A. Jahn, W.-J. J. Fischer, *Microelectron. Eng.* **2012**, *98*, 284.
- [34] T. D. B. Jacobs, T. Junge, L. Pastewka, *Surf. Topogr.: Metrol. Prop.* **2017**, *5*, 013001.
- [35] T. Endlein, A. Ji, S. Yuan, I. Hill, H. Wang, W. J. P. Barnes, Z. Dai, M. Sitti, *Proc. R. Soc. B* **2017**, *284*, 20162867.
- [36] E. V Eason, E. W. Hawkes, M. Windheim, D. L. Christensen, T. Libby, M. R. Cutkosky, *Bioinspiration Biomimetics* **2015**, *10*, 016013.
- [37] J. Y. Han, in *Proceedings of the 18th Annu. ACM Symposium on User Interface Software and Technology*, ACM Press, New York, NY **2005**, p. 115.
- [38] J. Schindelin, I. Arganda-Carreras, E. Frise, V. Kaynig, M. Longair, T. Pietzsch, S. Preibisch, C. Rueden, S. Saalfeld, B. Schmid, J. Y. Tinevez, D. J. White, V. Hartenstein, K. Eliceiri, P. Tomancak, A. Cardona, *Nat. Methods* **2012**, *9*, 676.
- [39] B. N. J. Persson, *Tribol. Lett.* **2014**, *54*, 99.
- [40] K. Brörmann, K. Burger, A. Jagota, R. Bennewitz, *J. Adhes.* **2012**, *88*, 589.
- [41] L. Afferrante, G. Carbone, *Macromol. React. Eng.* **2013**, *7*, 609.
- [42] Y. Y. Lin, C. Y. Hui, *Int. J. Fract.* **2004**, *126*, 205.
- [43] W. B. Dapp, A. Lücke, B. N. J. Persson, M. H. Müser, *Phys. Rev. Lett.* **2012**, *108*, 1.
- [44] K. Kendall, *J. Phys. D: Appl. Phys.* **1971**, *4*, 1186.
- [45] R. Spolenak, S. Gorb, H. Gao, E. Arzt, *Proc. R. Soc. A: Math. Phys. Eng. Sci.* **2005**, *461*, 305.